

# The 2007 rifting event in Northern Tanzania studied by C and L-band interferometry

A.M. Oyen<sup>a</sup>, C. Wauthier<sup>b,c</sup>, N. d'Oreye<sup>d</sup>

<sup>a</sup>Delft Institute of Earth Observation and Space Systems, Delft University of Technology, Kluyverweg, 1, 2629HS Delft, The Netherlands

<sup>b</sup>Royal Museum for Central Africa, Leuvensesteenweg, 13, 3080 Tervuren, Belgium

<sup>c</sup>Dept. ARGENCO, University of Liège, Sart Tilman B52, 4000 Liège, Belgium

<sup>d</sup>The National Museum of Natural History, Rue Josy Welter 19, 7256 Walferdange, G.D.-Luxembourg

---

## Abstract

July–August 2007, Lake Natron, Northern Tanzania. Part of the eastern branch of the East African Rift (EAR) is struck by a series of moderate earthquakes, culminating with a 5.9 Mw earthquake on the 17<sup>th</sup> of July 2007. Thanks to the co-operation of several teams, active in different areas of expertise, this earthquake swarm is recognised to be the first dyking event ever captured by space-borne remote sensing techniques as well as ground based measurements (Calais et al., 2008; Baer et al., 2008).

This study focuses on an in-depth analysis of the C and L-band interferograms covering this event by means of the two multi-acquisition InSAR approaches, proposed by Oyen et al. (2008). The supervised ambiguity cycle slip correction focuses on the correction of unwrapping errors in the interferogram. The second strategy, the multi-acquisition InSAR cascading based on numerical modelling, allows to combine interferograms from different acquisition geometries in order to improve the insights in certain complex geophysical phenomena, such as rifting events. The resulting, artificial interferograms with decreased temporal baselines show less complex deformation patterns and hence facilitate the interpretation of the deformation signal. The availability of L-band radar images, with higher coherence level and fewer phase cycles, significantly improved the interpretation. The residual interpretation of the models, however, has become more difficult compared to C-band.

*Key words:* East African Rift, continental rifting, radar interferometry, numerical modelling

---

## 1. Introduction

The East African Rift (EAR) is a North-South oriented geological feature that runs all the way through the African continent. The EAR is the result of continental stretching leading to the divergence of the African plate and is characterised by earthquakes and volcanism. This study focuses on the area in Northern Tanzania along the eastern branch of the rift. The area of interest contains a salt lake (the lake Natron) in the North-West and two main volcanoes (the Ol Doinyo Lengai and Gelai) located to the South and West of the lake respectively.

From July to August 2007 this area was struck by a seismic swarm centred on the southern flank of the Gelai volcano. The crisis was accompanied by renewed activity of the nearby Ol Doinyo Lengai volcano, with some unusual explosive eruptions in September 2007. This event was captured by GPS measurements, a local seismic network, and by two radar remote sensing instruments on the Envisat and ALOS satellites. The GPS station, located West of lake Natron, measured a displacement of approximately 5.6 cm vertically and 5.7 cm horizontally (Calais et al., 2008). This displacement was linked to the signal captured by the seismic network, but was much larger than expected at such a large distance from the earthquake's epicentres. The radar interferograms were able to reveal the size of the deformed area.

Based on the coherence level and deformation signal, eight potentially interesting interferograms from four different acquisition geometries are selected in Section 2 in order to analyse the observations. Amongst the selected interferograms, two in-

terferograms are acquired in L-band. The two multi-acquisition InSAR approaches, which are explored by Oyen et al. (2008), will be applied on this data stack in Section 4.

The results are discussed in Section 5. The supervised ambiguity cycle slip correction will be applied on two interferograms, one captured by the Envisat ASAR and one by the ALOS PalSAR instruments. The results of the multi-acquisition InSAR cascading approach based on numerical modelling indicate that this rifting event consisted out of several dyke intrusions on the central axis of the main graben. Furthermore, the results suggest that a magma-injection is preceded by slip on a fault plane located in the direction of the magma-displacements. Finally, some conclusions are drawn in Section 6.

## 2. Data availability

The Natron basin is monitored by both the Envisat ASAR and ALOS PalSAR instruments, providing a data set containing radar images from four different acquisition geometries. Amongst these, eight potentially interesting interferograms are selected to analyse the deformation pattern and its chronology. These interferograms, including a time line, are visualised in Fig. 1. The grey bar in the time line represents the total time span of the seismic swarm, while the red stars indicate the >5 Mw single events. Based on the acquisition dates of the available radar images, the seismic swarm is subdivided into three parts. *Part I* includes the deformation at the beginning of the seismic swarm (July 12–17). *Part II* represents the main part of the dyking episode (July 17 – August 21) and *Part III* represents the deformation after the 21<sup>st</sup> of August. The main shock on

July 17<sup>th</sup> is indicated by the red vertical bar in the time line, while the interferograms containing this earthquake are marked by a red box.

Based on seismic data and more interferograms not included in Fig. 1 no deformation is assumed before July 12<sup>th</sup> and after October 1<sup>st</sup>.

### 3. The supervised ambiguity cycle slip approach

High noise levels in interferograms can result in unwrapping errors. Unwrapping improvement can be applied by ambiguity cycle slip adjustment. The ambiguity cycle slips are detected by means of peak value detection in the gradient plots along the unwrapped interferogram in both East–West and North–South directions. The outliers, or the single pixels that are selected to be potential unwrapping errors, will be removed and the area to be corrected will be defined. This area will be shifted up or down with respect of the rest of the interferogram by  $2\pi$  or half the wavelength times an integer number. The term *supervised* refers to the use of a-priori information from other interferograms or geodetic measurements.

This approach is applied on interferograms 2:E(25697-28202) and 6:A(07727-09069). The corrected unwrapped interferograms are shown in Figs. 2 and 3. In both figures the black dots indicate the locations of the detected phase jumps. Moreover, these pixels are located in the graben area in both interferograms. It can be assumed that the deformation in graben areas is vertical (subsidence). This implies that the actual phase shift can be determined by cross-comparison of all the interferograms, rescaled to the vertical and temporal baseline, if necessary. Therefore, the interferograms are stacked and calibrated with respect to a chosen reference pixel with no deformation. The chosen pixel is located south-west of the lake Natron, where no deformation is assumed. The ambiguity number to correct for these cycle slips with is determined from a joint analysis of the cycle slip-free unwrapped interferograms and the field measurements.

Figs. 2 and 3 show that the ambiguity cycle slip adjustment is applied successfully. These optimised unwrapped interferograms will be used in the further analysis.

### 4. The multi-acquisition InSAR cascading approach based on numerical modelling

In order to improve the detailed analysis of some particular geophysical phenomena, geodetic observations are utilised as input for a modelling process. In the current study, InSAR data is used as input for a combination of the 3D Mixed Boundary Element Method (3D-MBEM) (Cayol and Cornet, 1996) and a near-neighbourhood algorithm (Sambridge, 1999a,b). The 3D-MBEM makes use of any type and number of user-defined sources. These sources are mainly fault planes with ‘slip’ or ‘opening’ or de/inflation sources. Furthermore, the 3D-MBEM method takes the topography into account, which avoids misinterpretation of the sources in mountainous areas, as is stated by Cayol and Cornet (1998).

In order to understand this continental rifting process in more detail, each interferogram, as presented in Fig. 1, will be simulated. Due to the large temporal sampling of the radar images, the complexity of the observed displacements of such geological events as observed in northern Tanzania is too high to provide accurate and realistic models of the traditional interferograms. Therefore, a method to decompose these displacements in smaller time periods has to be applied. The chosen method utilises several interferograms of different acquisition geometries with overlapping temporal baselines in order to create artificial, cascading interferograms.

This multi-acquisition InSAR cascading approach will be applied on *Part I*, *Part III*, and *Part II* respectively:

- *Part I* considers the deformation prior to the actual dyking episode and is fully contained in interferogram 1:E(26613-28116). The model of this interferogram is referred to as artificial interferogram 12072007-17072007.
- The modelling optimisation method for *Part III*, which represents the deformation after the dyking episode, will be applied as follows: the oldest interferogram 8:E(28703-29204) is modelled and subtracted from interferogram 7:E(28617-29619) in order to create the artificial interferogram 21082007-27082008.
- Subtracting the 12072007-17072007 deformation from interferogram 3:A(07253-07924) results in the artificial interferogram 17072007-21072007 or in *Part II<sub>a</sub>*. And, subtracting interferograms 4:E(28202-28703) and 21082007-27082008 results in interferogram 23072007-21082007 or *Part II<sub>c</sub>*. The remaining *Part II<sub>b</sub>* will be modelled by three artificial interferograms simultaneously.

The fringe discontinuities and linear oriented decorrelated pixels, that are observed in the wrapped interferograms and coherence image respectively, indicate the location of the surface ruptures and are confirmed by field observations. Combining the information of these three sources resulted in the fracture map as presented in Fig. 4. These fractures will be used in the modelling process.

According to the theory (Angelier et al., 1997) and the information resulting from the field observations (Delvaux et al., 2008), the geometry of the graben bounding faults is fixed during the modelling process. The dyke is assumed to be located on the central axis of the main graben and the graben bounding faults dip towards this central axis with a constant dip angle of 60°. The depth of the top of the dyke is determined by the depths of the bottom of the graben bounding faults. Moreover, the dyke is assumed to be vertical. Finally, the shear stress drops on deep buried faults is fixed at 3 MPa, while on the graben bounding faults a shear stress drop of 0 MPa is considered. The latter implies the passive nature of such faults as they are triggered by the stresses resulting from the dyke intrusion.

#### 4.1. Part I

*Part I*, which contains the deformation prior to the dyking episode, is modelled by a 9.7 km long normal fault. The fault

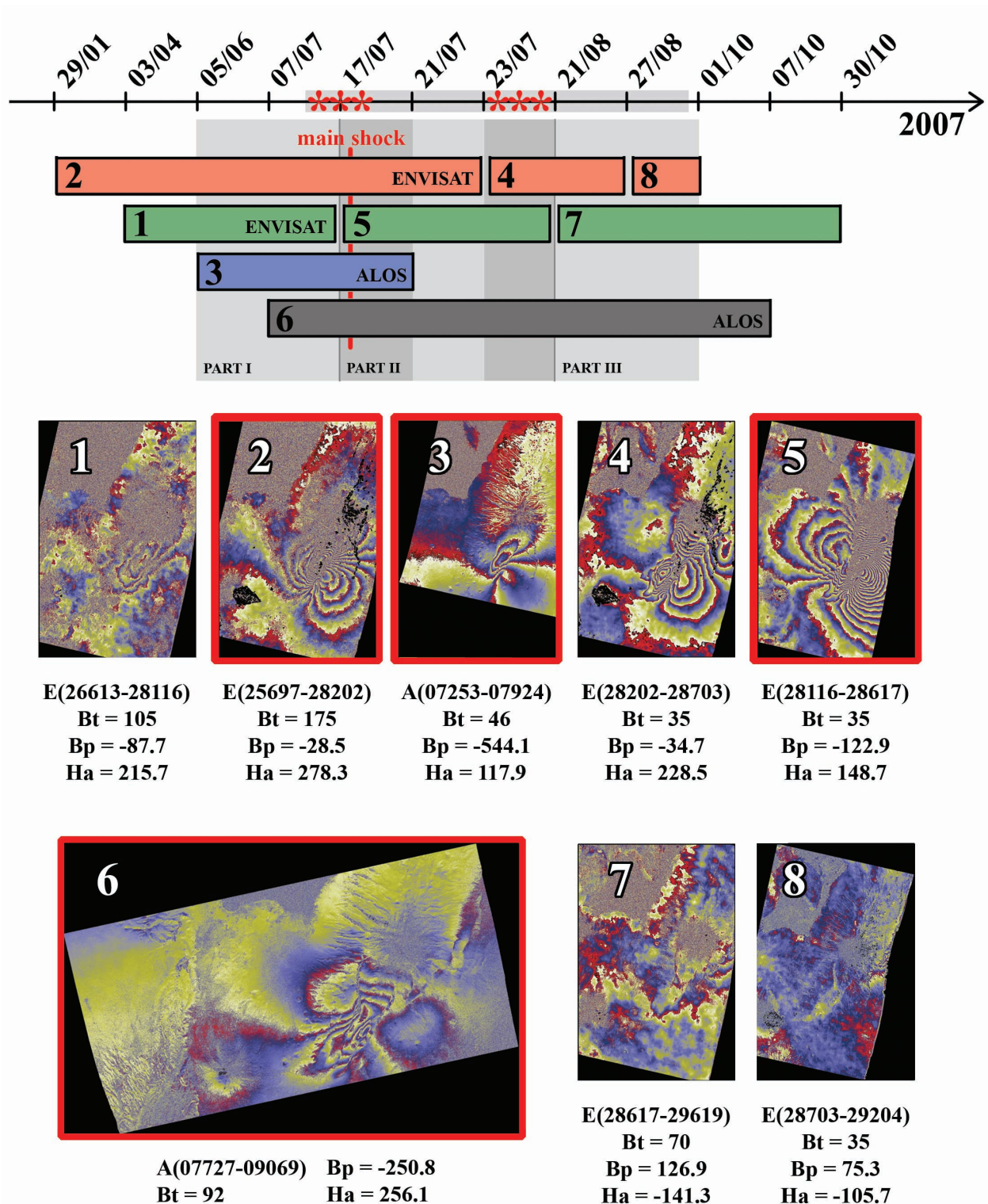


Figure 1: Summary of the differential interferometric results from 29/01/2007 to 30/10/2007. Green and red indicate respectively the Envisat track 6 (swath is6) and the Envisat track 92 (swath is2) interferograms. The descending and ascending ALOS interferograms are represented by blue and black respectively. Some important parameters of the interferograms, which are named by their respective orbit numbers, like temporal baseline ( $B_t$ ), perpendicular baseline ( $B_p$ ) and height ambiguity ( $H_a$ ) are listed next to each interferogram. The  $> 5$  Mw earthquakes of the seismic swarm, that started in the beginning of July 2007 and lasted up to September 2007, are indicated by the red stars on the time line. More specifically, the main shock is indicated by the vertical red line in the time line. The interferograms that contain this main shock are marked by the red boxes. The seismic swarm itself is indicated by the grey rectangle (July 2007 – September 2007).

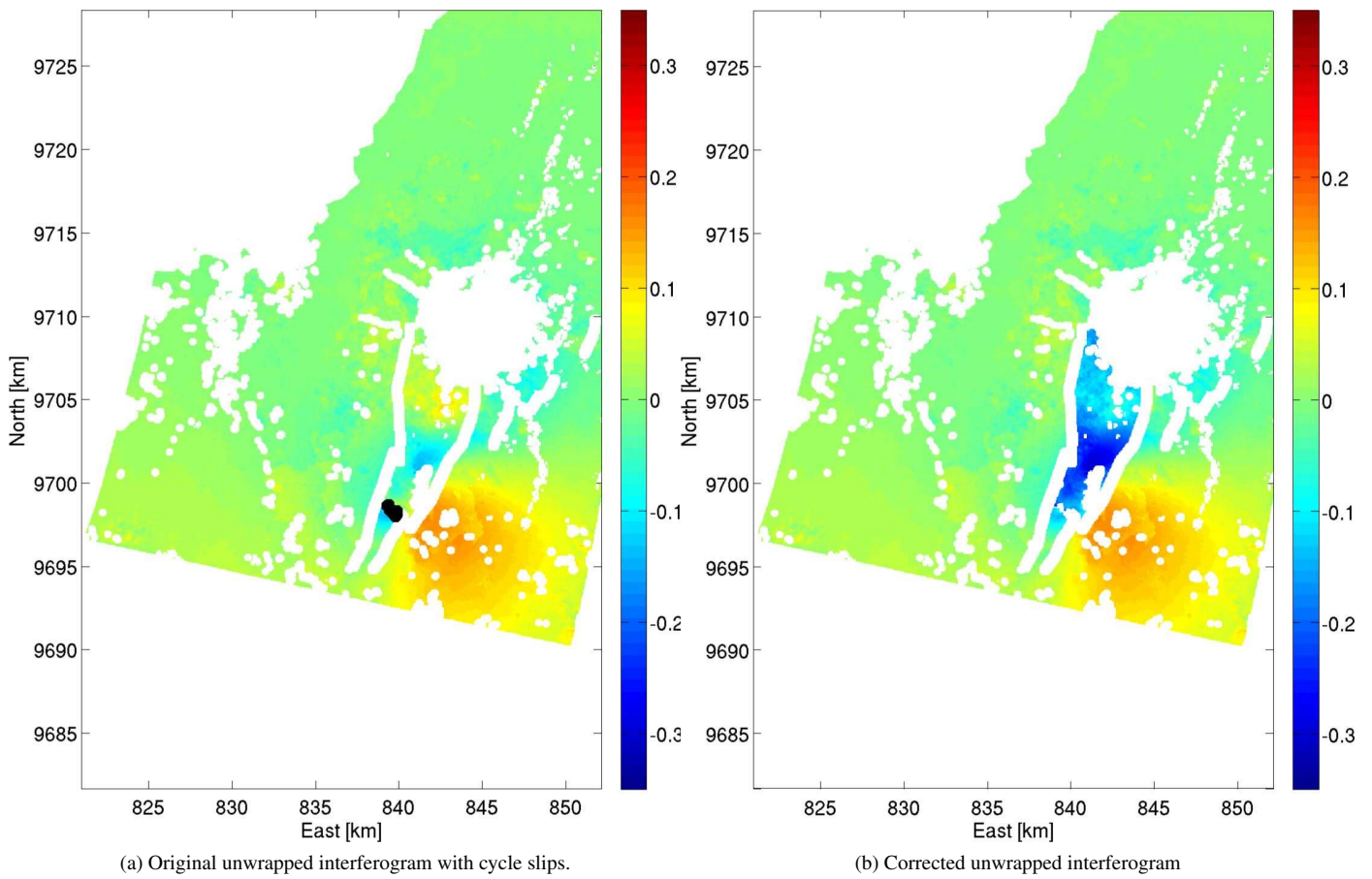


Figure 2: Unwrapping adjustment of interferogram 2:E(25697-28202). The values in both the colour bars are given in meters.

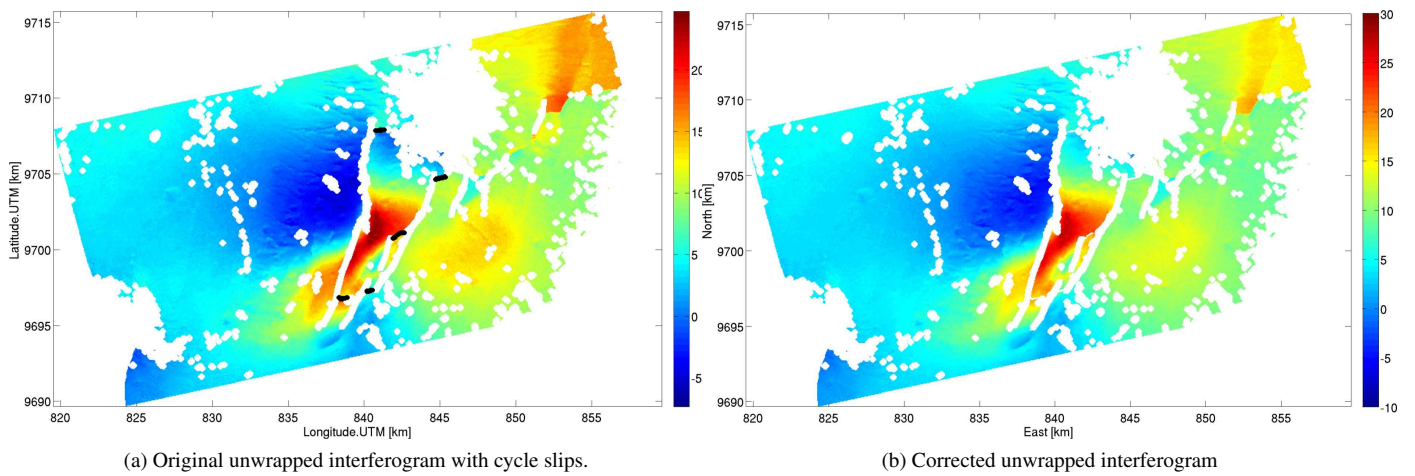


Figure 3: Unwrapping adjustment of interferogram 6:A(07727-09069). The values in both the colour bars are given in radian.

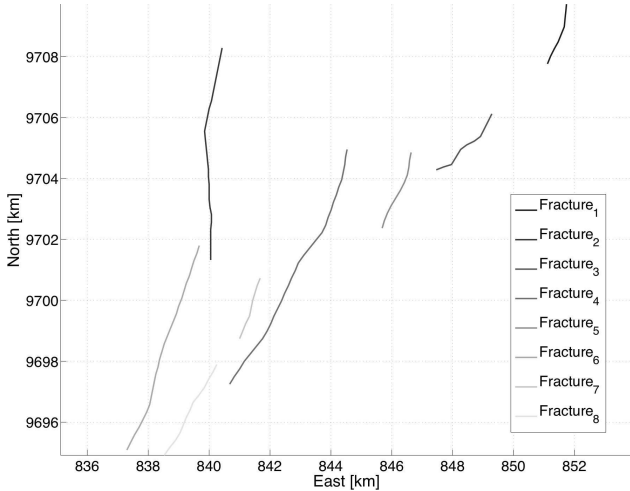


Figure 4: Mapping of the surface ruptures by cross-comparison of the coherence image and wrapped interferogram of interferogram 6:A(07727-09069) and field observations.

dips towards the northwest at an angle of  $54^\circ$  with an average slip of 1.5 m between depths of 4 km and 5.5 km below mean sea level (MSL). The dip and strike angle were determined by the seismic data as obtained by a local seismic network, (Calais et al., 2008). The model, referred to as interferogram 12072007-17072007, is shown in Fig. 6. The residual phases indicate that model simulates very well the observed displacements. The residual fringes are a result of atmospheric effects and are neglected in this study.

#### 4.2. Part II

The dyking episode is covered by *Part II* of the seismic swarm and is subdivided in three parts *a*, *b*, and *c*. Since no significant earthquake occurred between July 21 and July 23, both *Part II<sub>a</sub>* and *Part II<sub>b</sub>* are modelled simultaneous in order to get a more reliable model.

*Part II<sub>a</sub>* and *Part II<sub>b</sub>* contain the residual deformation of interferograms 2:E(25697-28202) and 3:A(07253-07924) and 12072007-17072007. The coherence image and the fringes in the wrapped interferograms indicate that Fracture<sub>4</sub> has reached the surface and some slip occurred on Fracture<sub>7</sub> and Fracture<sub>8</sub>. In order to simplify the model, the geometry of the graben bounding faults, i.e. Fracture<sub>2/4/7/8</sub>, is fixed. Furthermore, the model is created as a summation of two separated models: (i) one covering the dyke intrusion and the slip on the graben bounding faults and (ii) another one representing the slip on a normal fault plane, which corresponds to the 17/07/2007 main earthquake. The best fitting model suggests a dyke with an opening of 3 m at a depth of 2 km below MSL. The normal fault, associated to the main shock, has slipped 2 m in average at 3.4 km below MSL. The corresponding model is shown in Fig. 7. The residual phase in Fig. 7 indicate that the most of the observed displacements is

explained by the modelled sources. These sources are visualised in Fig. 8. However, the modelled displacements near the surface ruptures deviate from the observations. The residuals also show that the displacements inside the graben area are also underestimated.

*Part II<sub>c</sub>* covers the last phase of the dyking episode. During *Part II<sub>c</sub>* the western graben bounding faults, indicated by Fracture<sub>2</sub> and Fracture<sub>6</sub> in Fig. 4, as well as Fracture<sub>4</sub> have formed up to the surface. The model of that *part II<sub>c</sub>* is not yet considered in the present preliminary study.

#### 4.3. Part III

The interferograms covering *Part III* show few fringes of deformation on the eastern and southeastern flank of the Gelai volcano. Furthermore, some slight subsidence is observed in the main graben area, which can be linked to either visco-elastic relaxation of the earth or deformation due to the cooling down of the injected magma.

Interferogram 8:E(28703-29204) and interferogram 7:E(28617-29619) are both modelled by an east-dipping normal fault located on the southeastern flank of the Gelai volcano, with two superficial parts reaching the surface in Fracture<sub>1</sub> and Fracture<sub>3</sub> (see Fig. 4). Since interferogram 7:E(28617-29619) is easy to interpret and it fully covers the displacements mapped in interferogram 8:E(28703-29204), interferogram 8:E(28703-29204) will not be modelled in this study. However, in terms of chronology it is clear that the slip on the fault plane located on the southeast flank of the Gelai volcano migrated northwards.

The resulting model (Fig. 9) suggests an east-dipping fault with two superficial segments that reach the surface. The average slip on the fault is 4 cm. According to the residual phase in Fig. 9, the model explains the main fringe pattern southeast of the Gelai volcano. However, again the fringes near the surface ruptures are not perfectly reproduced by the model.

## 5. Discussion

In order to validate the results that are described in Section 4 they are compared to two existing studies performed on the same case study. Since both Calais et al. (2008) and Baer et al. (2008) made use of the Okada modelling technique it is not straightforward to make a comparison between the modelling results. The Okada method inverts the slip on individual patches along the fault and applies a certain smoothing factor, while the 3D-MBEM superimposes a homogeneous distribution of the shear stress drop on the whole fault plane and derives the global slip.

Calais et al. utilised the earthquake's epicentres to define a main fault plane and only takes into account interferograms 1:E(26613-28116) and 5:E(28116-28617). On the other hand, Baer et al. invert the position of numerous fault planes and apply a similar method to create artificial interferograms with decreased temporal baseline.

Another difference arises from the InSAR processing software used for these studies. Baer et al. applies software that makes use of the raw data provided by the instruments (the

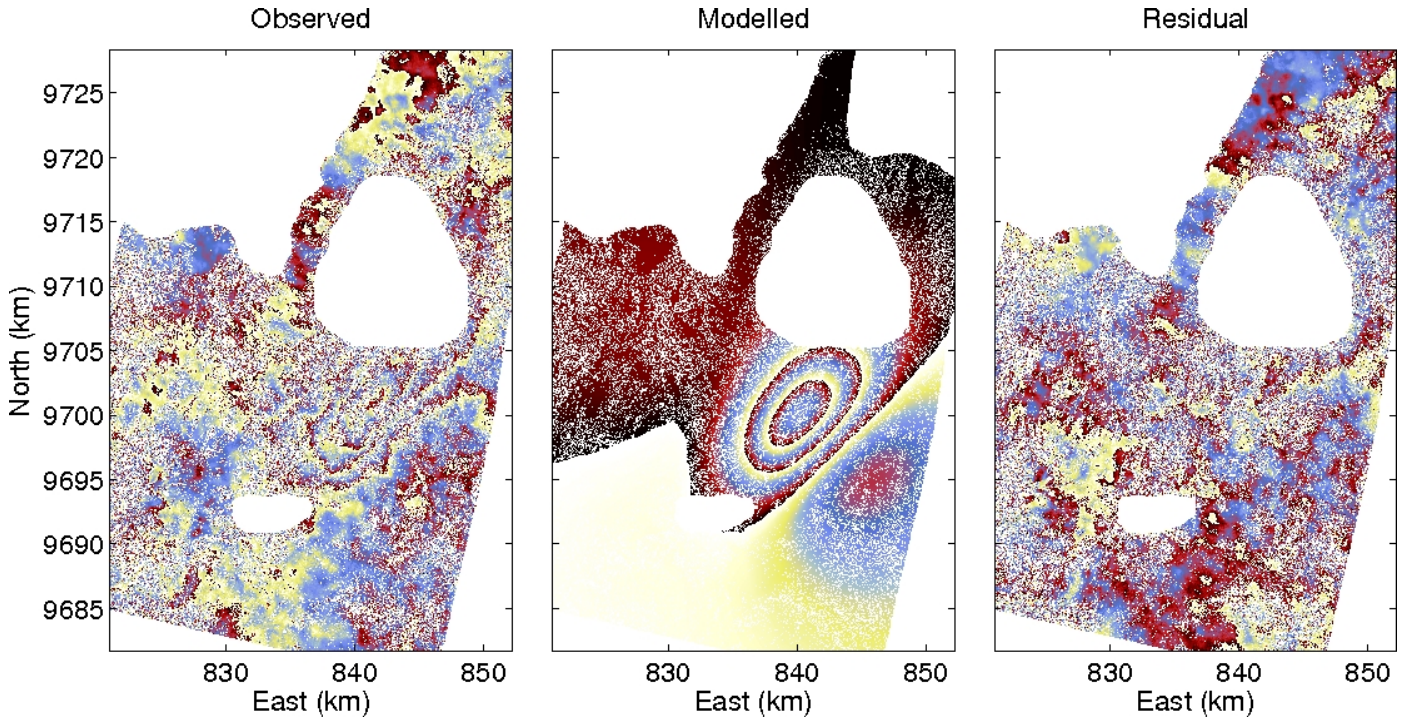


Figure 5: From left to right: observed deformation field from interferogram 1:E(26613-28116), best fit model, and residual displacements. (RMS: 11 mm)

JPL/Caltech ROI-PAC software and GAMMA software to perform the ALOS PalSAR processing). Like for the current study, Calais et al. used the open source DORIS software to process the C-band and L-band data. The DORIS software makes use of the so-called Level 1 data distributed by ESA, which are the focused single look complex data. As a result of the focussing algorithm used for that pre-processing by ESA, some data are lost near the edges of the radar images and the surface covered by the SAR images are slightly smaller. Since the Gelai volcano is located at the near range of the radar image, part of the displacements on the eastern flank of the Gelai volcano cannot be mapped.

### 5.1. Part I

Interferogram 1:E(26613-28116) is modelled in all studies by a west-dipping normal fault. Both Baer and Calais suggest a similar fault depth and length of 5–10 km and 32 km respectively. Both studies suggest a different slip of 30 cm and 50 cm respectively. This is due to the difference in orientation of the fault plane. The results presented here suggest a fault length of 9.7 km with an average slip of 1.5 m at a depth of 4.8 km below MSL. The suggested fault plane is slightly shallower and has a length and slip which are both approximately three times as much as in the former studies. This is mainly due to the difference in fault slip calculations of both the methods as stated earlier. The Okada method inverts the slip (expressed in meters) on the individual fault patches and applies a certain smoothing

factor. The 3D-MBEM superimposes a homogeneous distribution of the shear stress drop on the fault plane and derives the slip. In addition the topography has a large influence on the modelled displacements in this area.

### 5.2. Part II

The modelling would be more accurate and reliable when multiple observations, preferably from different acquisition geometries, are available. Therefore, interferograms 2:E(25697-28202) and 3:A(07253-07924) are modelled simultaneously as a single data set. This assumption is supported by the fact that Part II<sub>b</sub> spans only two days and no significant earthquakes occurred during that time.

The graben bounding faults are assumed to be fully triggered by the dyke intrusion, introducing the idea of passive faulting.

Baer et al. model Part II<sub>a/b</sub> as a combination of a dyke intrusion located in the southern part of the graben and slip on three fault planes. Two of these faults coincide with the graben bounding fault used in this study. The third fault plane is located below the Gelai volcano and corresponds to the main event on 17/07/2007. It has a length of approximately 7 km. The dyke has a length of 12 km and opens up to 1 m at a depth of 2 km. This study suggests a fault with similar length, but with a larger strike angle. The dyke has a length of 4.5 km but shows an opening of 2 m at a depth of 4.5 km. The difference between the results is remarkable in this stage. As it was the case in Part

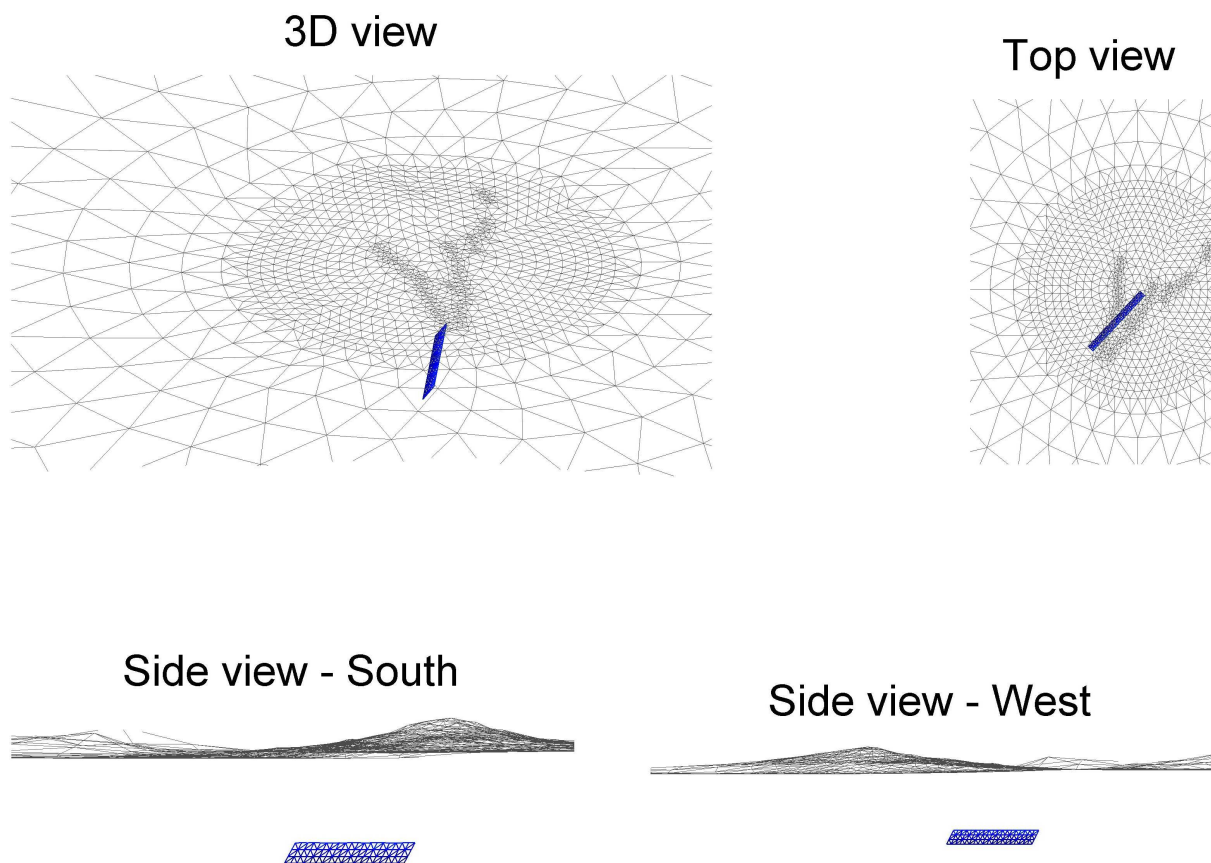


Figure 6: Interferogram 1:E(26613-28116): Sources.

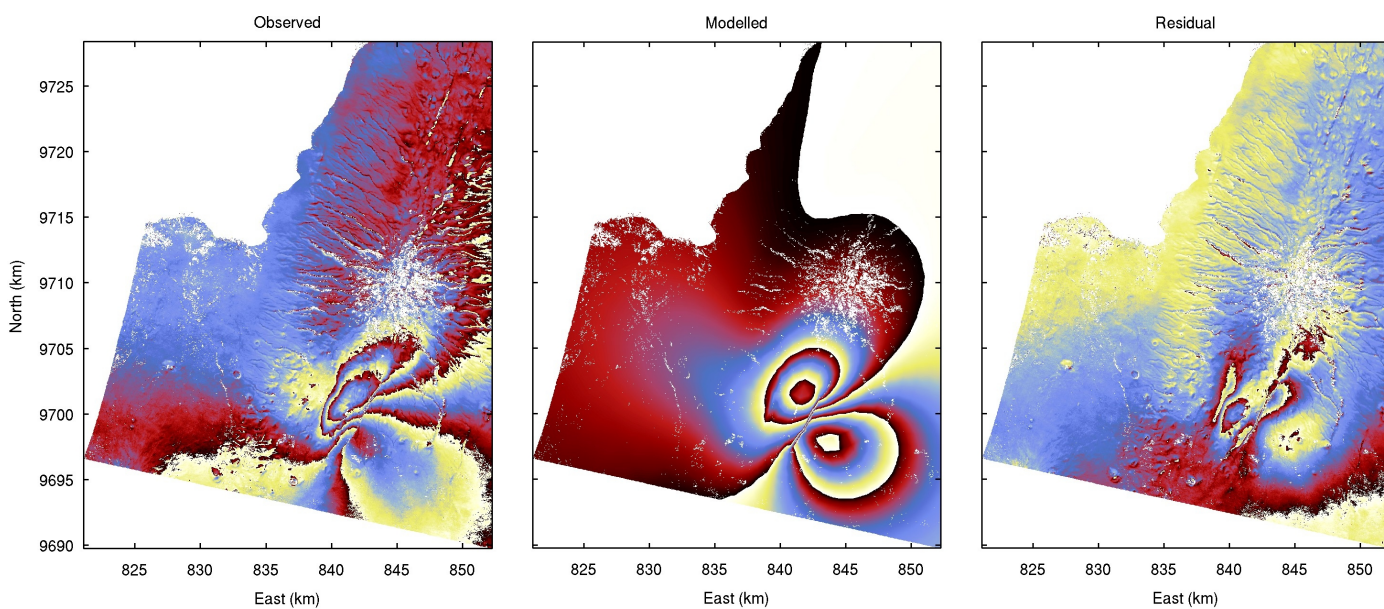


Figure 7: From left to right: observed deformation field from interferograms 2:E(25697-28202) and 3:A(07253-07924), best fit model, and residual displacements. (RMS: 37 mm)

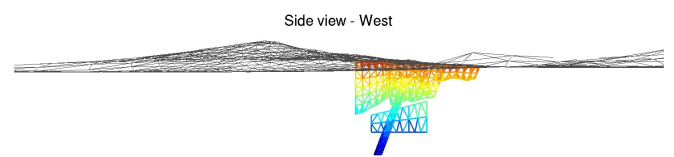
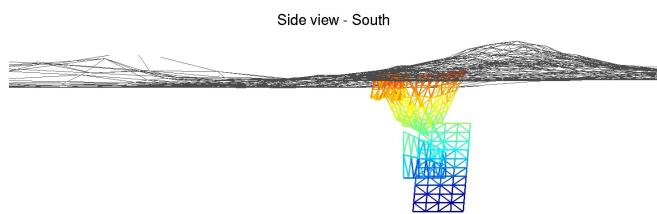
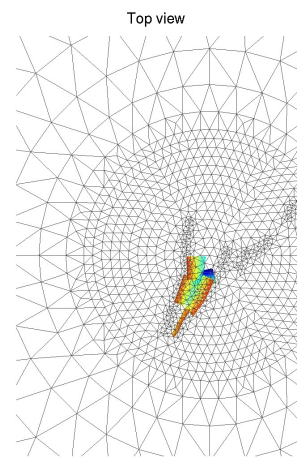
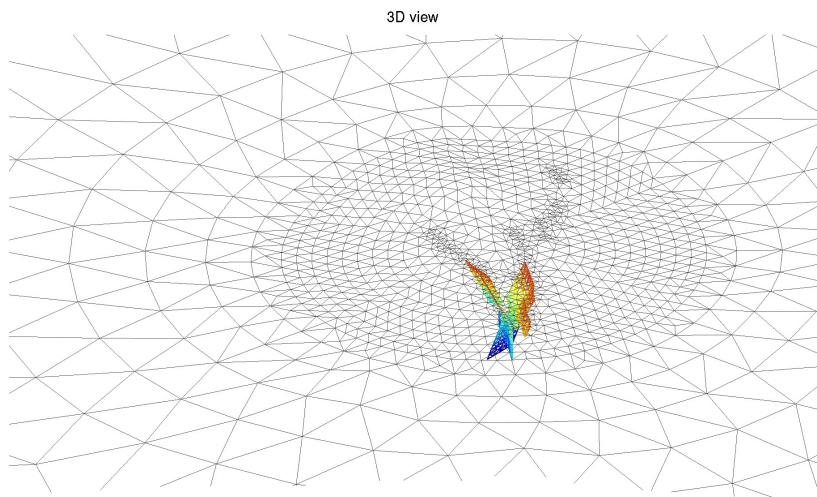


Figure 8: Interferograms 2:E(25697-28202) and 3:A(07253-07924): Sources.

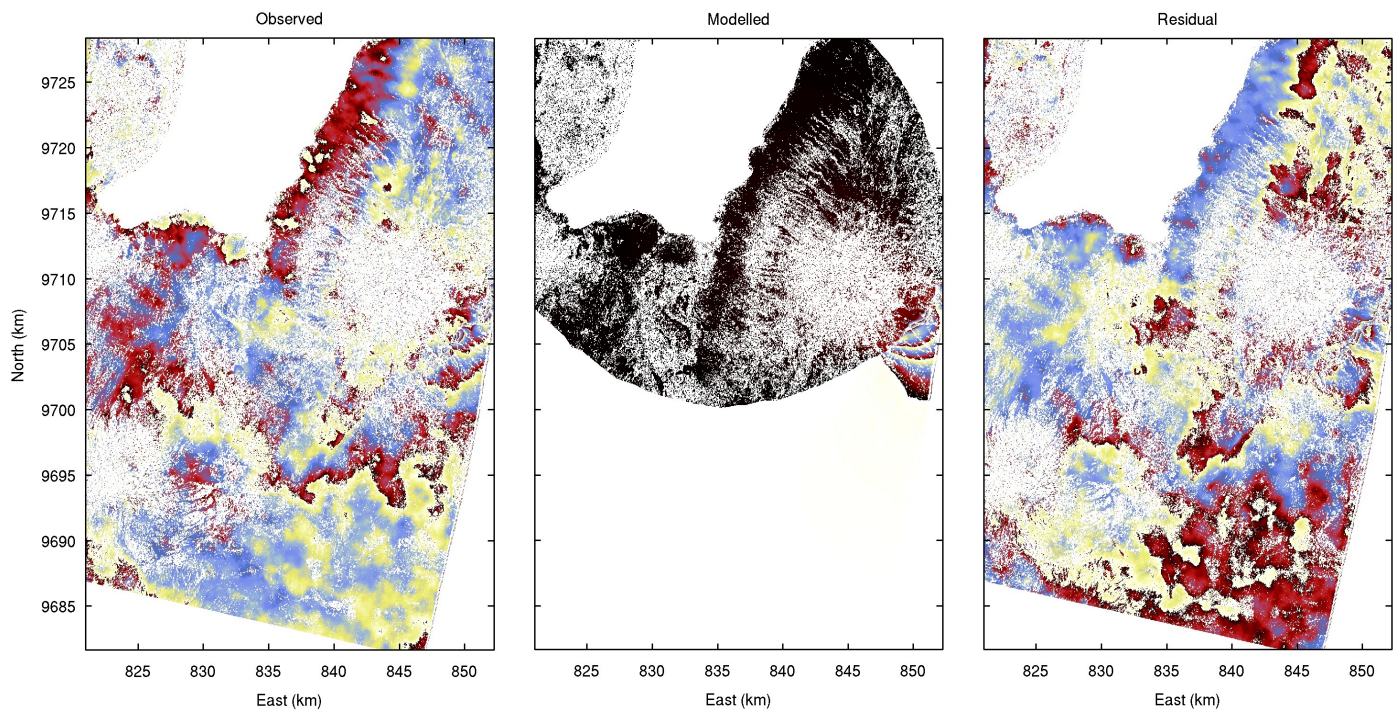


Figure 9: From left tot right: observed deformation field from interferogram 7:E(28617-29619), best fit model, and residual displacements. (RMS: 25 mm)

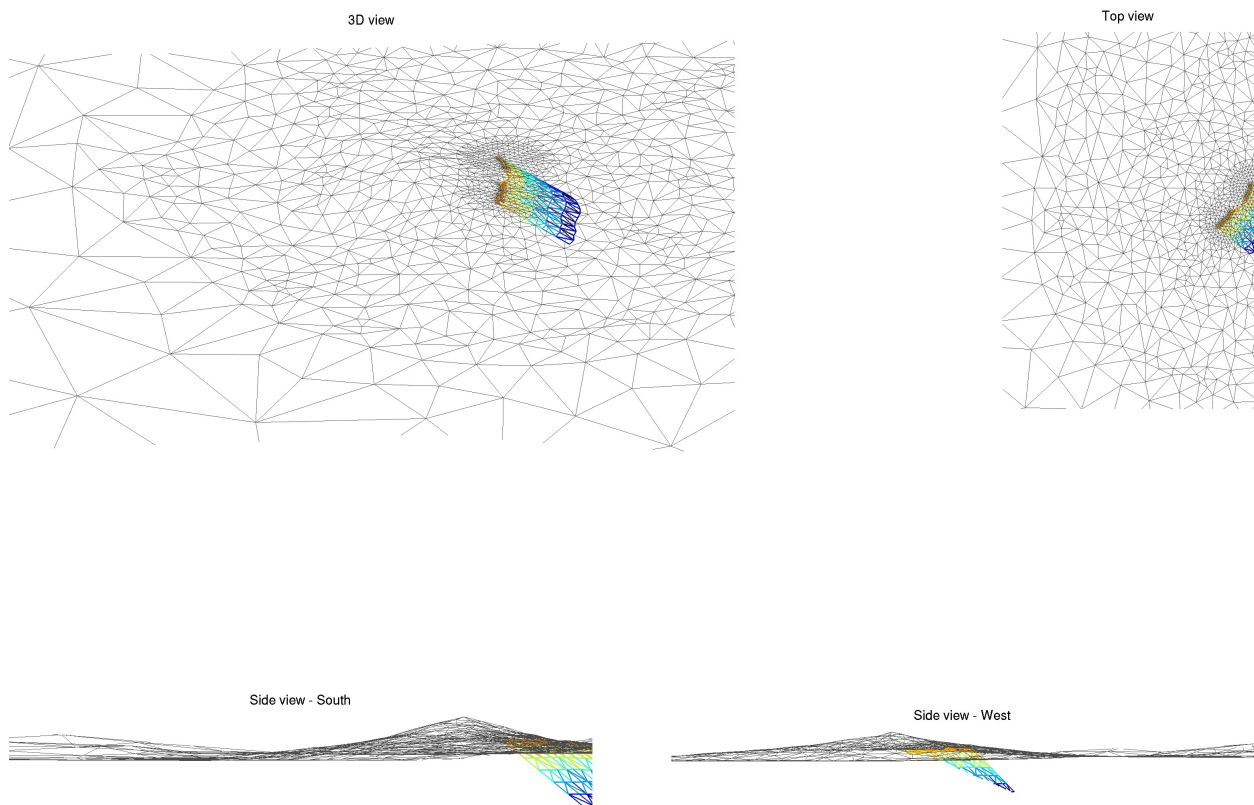


Figure 10: Interferogram 7:E(28617-29619): Sources.

I, this difference can be explained by the modelling techniques. The opening of the dyke intrusion as modelled by Baer et al. occurred in one main patch which is smeared out from north to south. The significant opening is only present in the northern half of the dyke. This reduces the length of the dyke to 6 km, which is closer to the result obtained by this study.

### 5.3. Part III

The deformation in both interferograms 7:E(28617-29619) and 8:E(28703-29204) is minor compared to that observed in the other interferograms. Therefore, Calais et al. did not consider these observations in the dyking episode analysis. Though, it is analysed by Baer et al.. According to their research, interferogram 7:E(28617-29619) can be modelled by 5 fault segments and a dyke intrusion at the location of Fracture<sub>2</sub>. Three of these faults are not detectable in our interferograms, and the graben is not considered in Part III of the swarm.

Therefore, it can be concluded that both studies agree on the location of the fault southeast of the graben. According to Baer et al., the maximum amount of slip is approximately 20 cm, which is twice the maximum slip on the fault plane modelled in this study. However, it is not clear on which of the 5 fault planes this maximum slip would occur in Baer et al.'s analysis.

## 6. Concluding remarks

This study applied both the supervised ambiguity cycle slip correction and the multi-acquisition InSAR cascading approaches (Oyen et al., 2008) to the 2007 Tanzanian seismo-magmatic event. It was concluded that the second proposed strategy facilitated the interpretation of the observed displacements. However, in terms of modelling the deformation observed in the artificial interferograms was not simplified up to the preferred level. Increasing the number of sources would increase the number of parameters to invert. Therefore, in the current study several assumptions were considered for the modelling. As outlined in Section 4, these assumptions were related to the geometry of the graben bounding faults and the dyke depth. The other assumptions are related to the shear stress drop superimposed on the faults. Depending on the kind of fault, the shear stress drop is adapted. It is kept constant at a value of 3 MPa for faults related to large earthquakes or 0 MPa for graben bounding faults and inverted over a range of 0–10 MPa for other types of faulting.

The interferograms that span both the period prior to the dyking episode and the dyking episode itself (Part I and Part II of the seismic swarm respectively) show a remarkable temporal pattern. The displacements in Part I are the result of slip along a fault plane located where the dyke intrusion modelled in Part II<sub>a/b</sub>. Furthermore, during Part II<sub>a/b</sub> and Part II<sub>c</sub> two west-dipping faults, located in the northern and southern part of the graben respectively, have slipped. This behaviour indicates the occurrence of fault slip prior to the dyke intrusion as a result of the stresses imposed by the upcoming magma.

Remarkable is the northward migration of fault motion on East-dipping faults on the southeastern flank of the Gelai volcano. A possible hypothesis of the driving forces triggering these faults is as follows. Since these faults are neither graben bounding faults nor faults indicating any dyke intrusion/migration, their orientation implies that it is very likely that they are a result of the remaining tensional forces in the earth's crust. Due to the large surface load implied by the Gelai volcano, it is not expected that any faulting would appear on the mountain flank. However, faulting is expected at the foot of the volcano, as is observed in these interferograms.

The dyking episode that occurred at the southern flank of the Gelai volcano in the summer of 2007 was accompanied by renewed activity of the Lengai volcano. The relatively small distance between the two volcanoes suggests a most probable link between the two events. Therefore, it is preferable to perform an InSAR time series analysis on the Lengai volcano in order to detect any deformation of the volcano or its surroundings prior to the dyking episode. Detecting such unusual behaviour of the earth's surface might help to predict new magmatic episodes and improve our knowledge about continental rifting.

Since the 3D-MBEM considers an elastic half space, the modelling of faults that reach the surface might be problematic. This is also observed in the models covering the dyking episode (Part II of the seismic swarm). An in-depth analysis the application of such faulting within the 3D-MBEM modelling method is also recommended.

## Acknowledgements

The radar images presented in this study are captured in the frame of the ESA Cat-1 project CT-3224 and the ESA-JAXA ALOS project 3690. The InSAR processing was performed by the DORIS software, developed by the Delft institute of Earth Observation and Space Systems (DEOS) of the Delft University of Technology (DUT). Orbital and topographic data are provided by DUT and SRTM respectively. The authors would like to thank P. Marinkovic for his assistance on the ALOS data processing and V. Cayol and Y. Fukushima for the use of the modelling codes and helpful suggestions.

## References

- Angelier, J., F. Bergerat, O. Dauteuil, and T. Villemin (1997). Effective tension-shear in extensional fissure swarms, axial rift zone of northeastern iceland. *Journal of Structural Geology*, 673–685.
- Baer, G., Y. Hamiel, G. Shamir, and R. Nof (2008, April). Evolution of magma-driven earthquake swarm and triggering of the nearby oldoinyo lengai eruption, as resolved by insar, ground observations and elastic modeling, east african rift, 2007. *Earth and Planetary Science Letters* 272(doi:10.1016/j.epsl.2008.04.052), 339–352. Issue 1-2.
- Calais, E., N. d'Oreye, J. Albaric, A. Deschamps, D. Delvaux, J. Déverchère, C. Ebinger, R. W. Ferdinand, F. Kervyn, A. S. Macheyeki, A. Oyen, J. Perrot, E. Saria, B. Smets, D. S. Stamps, and C. Wauthier (2008, December). Strain accommodation by slow slip and dyking in a youthful continental rift, East Africa. *Nature* 456(doi:10.1038/nature07478), 783–788.

- Cayol, V. and F. H. Cornet (1996). 3d mixed boundary elements for elastostatic deformation fields analysis. *Int. J. Rock Mech. Min. Sci. and Geomech. Abstr.* 34, 275–287.
- Cayol, V. and F. H. Cornet (1998). Effects of topography on the interpretation of the deformation field of prominent volcanoes - application to etna. *Geophysical Research Letters* 25, 1979–1982.
- Delvaux, D., B. Smets, C. Wauthier, and A. S. Macheyeki (2008). Brief scientific report of the october 2007 field work in northern tanzania. Field mapping of the surface ruptures associated to the July-August 2007 Gelai volcano-tectonic event.
- Oyen, A. M., P. Marinkovic, C. Wauthier, N. d'Oreye, and R. F. Hanssen (2008). A continental rifting event in Tanzania revealed by Envisat and ALOS InSAR observations. In *ALOS PI Symposium, Rhodes, Greece, 3–7 Nov 2008*, pp. 8.
- Sambridge, M. (1999a, March). Geophysical inversion with a neighbourhood algorithm - i: Searching a parameter space. *Geophysical Journal International* 138, 479–494.
- Sambridge, M. (1999b, April). Geophysical inversion with a neighbourhood algorithm - ii: Appraising the ensemble. *Geophysical Journal International* 138, 727–746.